Direct calculation of interfacial tensions from computer simulation: Results for freely jointed tangent hard sphere chains

Luis G. MacDowell
Departamento de Química Física, Facultad de Ciencias Químicas, Universidad Complutense de Madrid, 28040, Spain

Paweł Bryk
Department for the Modeling of Physico-Chemical Processes, Maria Curie-Sklodowska University, 20-031 Lublin, Poland
(Received 27 February 2007; revised manuscript received 29 April 2007; published 29 June 2007)

We develop a methodology for the calculation of surface free energies based on the probability distribution of a wandering interface. Using a simple extension of the *NpT* sampling, we allow the interface area to randomly probe the available space and evaluate the surface free energy from histogram analysis and the corresponding average. The method is suitable for studying systems with either continuous or discontinuous potentials, as it does not require explicit evaluation of the virial. The proposed algorithm is compared with known results for the surface tension of Lennard-Jones and square well fluids, as well as for the interface tension of a bead-spring polymer model, and good agreement is found. We also calculate the interfacial tensions of freely jointed tangent hard sphere chains on athermal walls for a wide range of chain lengths and densities. The results are compared with three different theoretical approaches: scaled particle theory (SPT), Yu-Wu density functional theory, and an analytical approximation based on the latter approach. Whereas SPT only yields qualitative results, the last two approaches are found to yield very good agreement with simulations.

DOI: 10.1103/PhysRevE.75.061609 PACS number(s): 68.03.Cd, 68.08.−p, 68.35.Md

I. INTRODUCTION

Interfacial phenomena have been a matter of great research interest for centuries [1]. With the growing importance of nanotechnology, however, this field of research is expected to become even more relevant. As the surface-to-volume ratios diminish in miniaturized devices, surface effects become increasingly important and strongly influence the state of the systems [2], including new and surprising behavior [3,4].

Whereas the structure of the interface can be quite complex at the microscopic level [5–11], from a thermodynamic point of view only the interfacial tensions are really required to describe the system's behavior in most instances (e.g., Young's equation). Statistical mechanics provides a link for the calculation of interface tensions in terms of the average of a mechanical property: namely, the anisotropy of the pressure tensor [12]. This route has been applied to estimate interface tensions, either theoretically [1] or by means of computer simulations [13]. Results are known for some prototype systems, including the Lennard-Jones [14], square well [15], and Gay-Berne [16] fluids, as well as bead-spring polymer chains [17–19]. Unfortunately, the explicit evaluation of the pressure tensor is already a very subtle matter for simple fluids [1,17]. The presence of discontinuities in the potential, either inherent in the model or resulting from truncation in computer simulations can cause difficulties [14] and, at any rate, need the approximate evaluation of Dirac δ functions. For molecular fluids the difficulties may become even more important, since the bonding is often rigid and the resulting contribution of the constraining forces becomes difficult to estimate [18,19].

Several methods have been proposed in the literature to overcome the difficulties related to explicit evaluation of the virial. A useful methodology which is particularly interesting in the vicinity of the critical point was proposed long time ago by Binder [20] and has received renewed interest recently [9,21,22]. Although cast in terms of probability distributions, this method is equivalent to a full thermodynamic integration from the one-phase state to a two-phase state [23]. In that sense, it can be considered as an extension of thermodynamic integration employed to calculate interfacial tensions from adsorption isotherms [24]. The need for sampling all states between the homogeneous bulk phase and the phase coexisting states (slab geometry) makes it fairly time consuming away from the critical point. On the other hand, one gets a large amount of information on the intermediate metastable states which can be exploited for use in nucleation studies [25,26]. Alternatively, one can explicitly simulate two-phase states only and attempt to collect averages containing information on the interface. One such method is based on the capillary Hamiltonian approximation, whereby the spectra of interfacial capillary waves are analyzed, and the surface tension is obtained from the long-wavelength behavior [9,18,27]. This method may be applied only for the liquid-vapor interface and presents difficulties related to the explicit location of the interface boundary, but does not seem to be affected by this arbitrariness at long wavelengths [28]. A third route that allows one to calculate interfacial tensions without explicit evaluation of the virial is based on the perturbation of the two-phase system, by increasing or decreasing the interface a finite amount. For curved interfaces, this method resembles the philosophy of scaled particle theory [29–31] and was exploited by Bresme and Quirke in order to calculate the interfacial tension of colloidal nanoparticulates [32,33]. Another perturbative approach, the test area method of Gloor *et al.*, has been recently applied to the study of flat interfaces, providing reliable estimates for spherical and an-

isotropic fluids [34,35]. These methods are special cases of a more general methodology which can be applied to measure first derivatives of the free energy [36], with the Widom test particle method as the most widely known application [37]. In the perturbative methods, the difficulty is the choice of surface increment and a reliable average of the resulting small energy change, as is the case in the evaluation of numerical derivatives. In this work we propose a method which has features of both the Binder method, in the sense that it relies on histogram analysis, and the perturbative approaches employed by Bresme and Quirke and Gloor *et al.*, in the sense that the system is subject to small perturbations of the surface area. The difference is that the perturbations add up and the interface is allowed to wander freely. An analysis of the resulting probability distribution, or, alternatively, the corresponding average, yields the required interface tensions.

Another route for calculating the interfacial tension is density functional theory. In this approach the grand potential of the system is a functional of the local density; therefore, the interfacial tension is readily accessible once the functional is minimized. Several density functionals and related self-consistent field theories for polymeric fluids have been proposed in the literature [8,38–40]. One class of functionals is based on the polymer reference interaction site model [24,38,41,42]. Another class is based on the Woodward formalism [8,43,44]. In this work we use the functional belonging to the latter class and proposed by Yu and Wu [43]. This theory is based on Wertheim's first-order thermodynamic perturbation theory [45] (TPT1) and is one of the most accurate functionals for tangent hard sphere systems. However, besides the comparison with our simulation methodology, our choice of the functional serves another purpose. The Yu-Wu theory is also used as a starting point for the derivation of an analytical approximation for the interface tension of tangent hard sphere chains at hard walls. This simple approximation will turn out to be in a good agreement with the simulation data.

The content of the paper is organized as follows. In next section we briefly consider the surface thermodynamics of systems with inhomogeneous density profiles along one direction perpendicular to the interface. This is applied for the two cases of interest: free liquid-vapor interfaces and fluid-substrate interfaces. Having considered these formal aspects, we present the method proposed for the calculation of interface tensions in Sec. III. Results for the different systems studied, from the Lennard-Jones fluid to athermal chains are presented in Sec. IV, where a comparison is made to density functional theory (DFT) results and scaled particle theory. Finally, Sec. V presents our conclusions.

II. SURFACE THERMODYNAMICS OF SLIT PORE GEOMETRY

In this section we will study the thermodynamics of systems having an inhomogeneous interface profile along a single direction z. This includes two systems of interest, among others. One consists of (say) a liquid slab surrounded by vapor (or any other coexisting phase) in a system with periodic boundary conditions in all three directions. The other is a fluid in contact with a substrate, with periodic boundary conditions only in the directions perpendicular to z. For the sake of generality, let the container have orthogonal shape, with sides of length L_x, L_y, and L_z (note that in a slit pore the choice of L_z amounts to an arbitrary definition of the dividing surface). Work can be done on the system by changing the shape in either of two ways. First, one can perform displacements of the xy plane along the perpendicular direction. Let $p_\perp$ be the external pressure exerted on this moving plane. The work done by an infinitesimal increment of L_z is then given by $dw=-L_xL_yp_\perp dL_z$. Alternatively, one can perform perpendicular displacements of the yz and zx planes, thereby producing an infinitesimal increment of the xy plane. The resulting amount of work is then $dw=-L_zp_\parallel d(L_xL_y)$, where $p_\parallel$ is the average external pressure exerted on the yz or zx planes:

$$p_\parallel = \frac{1}{L_z}\int \frac{1}{2}[p_{xx}(z)+p_{yy}(z)]dz. \tag{1}$$

Accordingly, we may write for the infinitesimal changes in energy

$$dU = TdS - Ap_\perp dL_z - L_zp_\parallel dA + \mu dN, \tag{2}$$

where $A=L_xL_y$. Introducing a grand potential by means of the Legendre transform $\Omega=U-TS-\mu N$ yields

$$d\Omega = -SdT - Nd\mu - Ap_\perp dL_z - L_zp_\parallel dA. \tag{3}$$

In practice, we will be concerned with deformations which preserve the volume, hence $AdL_z+L_zdA=0$. It then follows that

$$\left(\frac{\partial\Omega}{\partial A}\right)_{\mu VT} = -L_z(p_\parallel - p_\perp). \tag{4}$$

In the limit of large L_z, where the two interfaces do not interact any longer, the above derivative is identified with twice the interface tension γ_∞. For the more general case where interaction among the interfaces is possible, we may therefore write

$$d\Omega = -SdT - Nd\mu + 2\gamma(L_z)dA. \tag{5}$$

Note that Ω is a first-order homogeneous function of the interface area cf. [Eq. (3)]. This allows us to write

$$\Omega = 2\gamma A - p_\perp AL_z. \tag{6}$$

This equation will be exploited later on in order to calculate γ.

In order to make contact with the standard thermodynamics of slit pores, two new definitions must be introduced. First, a solvation force is defined as the excess of $p_\perp$ over the expected bulk pressure $f_s(L_z)=p_\perp-p$. Second, we introduce a surface free energy per unit area, $2\omega(L_z)=-(p_\parallel-p)L_z$. With these definitions, Eq. (3) then becomes

$$d\Omega = -SdT - pdV - Nd\mu + 2\omega dA - Af_sdL_z. \tag{7}$$

The resemblance with the thermodynamics of slit pores is now apparent, although the volume here is just that of the actual system, $V=L_xL_yL_z$, with no mention of the reservoir. The equivalence of the two descriptions follows by consid-

ering the surface excess free energy. The free energy increment of a bulk system of equal shape and size is readily obtained either from Eq. (3) after replacement of N, S, and $p_{\parallel}$ and $p_{\perp}$ with the corresponding bulk values or from Eq. (7) by retaining the first three terms on the right-hand side. In either case, we obtain the excess free energy differential that is standard in slit pore thermodynamics [46]:

$$d\Delta\Omega_{ex} = -\Delta S_{ex} dT - \Delta N_{ex} d\mu + 2\omega dA - A f_s dL_z, \quad (8)$$

where the subscript ex stands for excess amounts over the corresponding bulk property.

Whether one uses Eq. (3) or Eq. (7) as the fundamental relation is just a matter of convenience. In experimental work on slit pores, one has control over L_z, A is difficult to modify, and Eq. (7) is more convenient. In the case of the simulations performed in this work, Eqs. (3) and (5) will prove more useful since only the independent variables are made explicit and none of these refer to the reservoir, which cannot be actually simulated. Furthermore, we expect $\gamma(L_z)$ to converge fast. Indeed, to a good approximation the difference between $\gamma(L_z)$ and γ_∞ arises from contributions well inside the infinitely large slit where $p_{\parallel}-p_{\perp}$ is zero anyway.

III. METHOD FOR THE CALCULATION OF INTERFACIAL TENSIONS

A. Formal aspects

The method proposed is conceptually very simple and resembles other known methods where the simulation's box shape is allowed to fluctuate [47–50]. In the absence of any other constraint, the shape of the system at fixed temperature, chemical potential, and volume will result from a competition between $p_{\parallel}$ and $p_{\perp}$. The rules of this competition are dictated by a probability density $f_{\mu VT}(A)$ and the corresponding free energy as follows:

$$\Omega_{\mu VT}(A) = -k_B T \ln f_{\mu VT}(A). \quad (9)$$

This provides the link between the statistical mechanical property f and the macroscopic observables. By use of Eq. (6), we find right away

$$f_{\mu VT}(A) = e^{-\beta(2\gamma A - p_{\perp} V)}. \quad (10)$$

This is the key result of the method proposed: sampling the interface at constant volume from the above distribution will readily yield the interfacial tension. For systems where the interfaces do not interact and both γ and $p_{\perp}$ are system size independent, it is clear that the slope of $\ln f_{\mu VT}$ yields the interfacial tension right away. For finite systems $f_{\mu VT}$, the analysis is complicated by the nontrivial dependence of $\gamma(L_z)$ and also $p_{\perp}(L_z)$. If sufficiently fine data are available, however, one can still recover $\gamma(L_z)$, since, according to Eqs. (5) and (9), we have

$$\frac{1}{f}\left(\frac{\partial f}{\partial A}\right)_{\mu VT} = -2\beta\gamma(L_z). \quad (11)$$

In practice, however, Eq. (10) as stated above is hardly useful, because $f_{\mu VT}(A)$ is a monotonous function; i.e., the unconstrained system does not have an equilibrium state and during a simulation it will either stretch infinitely in order to eliminate the interface if γ is positive or increase its lateral size continuously if γ is positive.

In order to overcome this difficulty, two different solutions seem possible. One is to add an extra work contribution that counterbalances the interfacial tension (balance sampling), yielding a proper equilibrium state. The other one is to constrain the system's area within a bracketed interval chosen conveniently (bracketed sampling). In practice, both physical situations amount to the introduction of a modified or constrained probability density of the form

$$\tilde{f}_{\mu VT}(A) = e^{-\beta W(A)} f_{\mu VT}(A), \quad (12)$$

where $W(A)$ is a suitably chosen function of A.

This distribution may be obtained from knowledge of the molecular interactions by sampling a modified grand canonical probability density of the form

$$\tilde{f}_{\mu VT}(N,A;\{\mathbf{r}\}_N) \propto e^{\beta\mu N} e^{-\beta\{\mathcal{U}[\{\mathbf{r}\}_N]+W(A)\}}, \quad (13)$$

where $\mathcal{U}$ is the intermolecular potential energy and $\{\mathbf{r}\}_N$ is the set of position vectors that define the microstate of a system with overall N molecules. An obvious choice for the evaluation of the above probability density is the standard grand canonical Monte Carlo method, with the addition of an extra box shape sampling. The box shape sampling is performed in the same spirit as in the standard NpT simulations. Each position vector $\mathbf{r}_i=(r_x,r_y,r_z)$ is transformed into a dimensionless position vector $\mathbf{t}_i=(r_x/L_x, r_y/L_y, r_z/L_z)$, and the relevant density distribution to sample the shape of the simulation box becomes

$$\tilde{f}_{\mu VT}(N,A;\{\mathbf{t}\}_N) \propto e^{\beta\mu N} V^N e^{-\beta\{\mathcal{U}[\{\mathbf{t}\}_N;L_x,L_y,L_z]+W(A)\}}, \quad (14)$$

where we have made explicit the parametric dependence of the intermolecular energy on the box shape that results from the transformation.

B. Practical implementation

In this section we discuss the implementation of the proposed method using Monte Carlo simulations for the sampling of Eq. (13). Other possible choices such as the Wang-Landau sampling [51] and molecular dynamics will not be discussed here but are also possible.

A simulation box of suitable size is chosen with initial values of $L_z=D$ about twice those of $L_x=L_y=L$. The simulation is then carried out using a standard grand canonical method, organized in cycles of several regular canonical and grand canonical trials. After the end of each cycle, a box deformation is attempted as follows. First, an area increment Δ is chosen uniformly from the interval $[-\Delta_{max},\Delta_{max}]$ and a new trial area $A_n=A_o+\Delta$ is proposed. The new box parameters are set accordingly as $L_n=A_n^{1/2}$ and $D_n=V/A_n$. The attempted move is then accepted with probability

$$P_{accept} = \min(1, e^{-\beta(\mathcal{U}_n-\mathcal{U}_o+W_n-W_o)}). \quad (15)$$

Obviously, the choice of W is a crucial issue for the performance of the method. At first sight, a work contribution that

competes against the γA term so as to produce a well-defined equilibrium state seems the most appropriate. Unfortunately, due to the small systems considered, the equilibrium value of A must fall within a fairly limited interval. Whereas this can be achieved in principle, in practice it amounts to good *a priori* knowledge of γ. Therefore, after several attempts with possible W functions, it was found that the most convenient procedure is simply to bracket the interface area within an interval chosen beforehand, by means of the following W function:

$$e^{-\beta W(A)} = \begin{cases} 0, & A < A_{min}, \\ 1, & A_{min} < A < A_{max}, \\ 0, & A > A_{max}. \end{cases} \tag{16}$$

Within the chosen interval, the method produces the probability distribution of Eq. (10). For noninteracting interfaces, a logarithmic plot of $f_{\mu VT}(A)$ yields the interfacial tension right away, while for interacting interfaces, Eq. (11) would have to be employed in order to determine $\gamma(L_z)$. In the former case, routine calculation of interfacial tensions may become somewhat cumbersome and a simpler data analysis might be desirable. One such possibility is to exploit the expectation value of the surface area, which reads

$$\frac{\langle A \rangle - A_{1/2}}{\Delta A} = \frac{1}{2\beta\gamma\Delta A} - \frac{1}{2}\frac{1+e^{-2\beta\gamma\Delta A}}{1-e^{-2\beta\gamma\Delta A}}, \tag{17}$$

where $\Delta A = A_{max} - A_{min}$ and $A_{1/2} = 1/2(A_{max} + A_{min})$. The root of the above equation is the maximum-likelihood estimate of γ given $\langle A \rangle$ and may be solved by means of a Newton-Raphson method. The first-order solution $2\beta\gamma\Delta A = 12(A_{1/2} - \langle A \rangle)/\Delta A$ may be used as an excellent first guess, producing convergence in less than four iterations. In fact, this approximation is good in most practical situations, as it produces deviations that are less than 3% from the exact solution for values of $(A_{1/2} - \langle A \rangle)/\Delta A$ in the range $[-0.1, 0.1]$.

So far, the methodology described applies for calculation of interfacial tensions in an open system. The choice of variables μ, V, and T is appropriate for calculating tensions of a fluid against a wall. Interfacial tensions between two coexisting phases are also of great importance, but the thermodynamic description employed here is not applicable right away. An initial state with two such phases will spontaneously transform into one or the other phase and completely eliminate the interface. This problem is solved immediately simply by replacing μ with N as the natural variable, with the number of particles fixed within the immiscibility gap. The entire framework that was employed in this section is then immediately applicable by simply replacing the grand free energy by the Helmholtz free energy and ignoring the sampling over the particle number.

IV. MODEL AND RESULTS

A. Molecular Models Studied

The bracketed interfacial area sampling described in the previous section will be applied to the study of four different systems. First, we will consider an argonlike model, with pair interactions that only depend on the mutual distance r between the atoms and obey the usual Lennard-Jones (LJ) potential

$$V_{LJ}(r) = 4\epsilon\left\{\left(\frac{\sigma}{r}\right)^{12} - \left(\frac{\sigma}{r}\right)^{6}\right\}. \tag{18}$$

Second, a central force potential of the square well type will also be considered:

$$V_{SW}(r) = \begin{cases} \infty, & r < \sigma, \\ -\epsilon, & \sigma \leqslant r < \lambda\sigma, \\ 0, & r \geqslant \lambda\sigma, \end{cases} \tag{19}$$

where λ defines the width of the square well and σ and ϵ are the usual range and energy parameters of the models.

Third, we will consider a well-known bead-spring polymer model which has been extensively studied. In this model, all beads interact with each other, whether in the same or different polymer, by means of a truncated and shifted Lennard-Jones potential with $R_c = 2 \times 2^{1/6}\sigma$. Additionally, adjacent beads within the same polymer are held together by means of a finite extensible nonelastic (FENE) potential of the form

$$\Phi(r) = -k_s R_\infty^2 \ln\left(1 - \frac{r^2}{R_\infty^2}\right), \tag{20}$$

where $k_s = 15\epsilon/\sigma^2$ plays the role of spring constant and $R_\infty = 1.5\sigma$ is the maximum allowed displacement between bonded beads. Whereas for the simple atomic fluids only the vapor-liquid interfacial tensions will be calculated, for the polymer we will also report wall-fluid interface tensions. The polymers will thus be confined between two parallel plates in the usual slit pore geometry, with fluid-substrate interactions of the form

$$V_{wall}(z) = A\left\{\left(\frac{\sigma}{z}\right)^{9} - \left(\frac{\sigma}{z}\right)^{3}\right\}, \tag{21}$$

where A plays the role of a Hamaker constant.

The last model considered in this work will be a chain of freely jointed tangent hard sphere chains. In this case, beads interact with each other via a hard sphere potential of the form

$$V_{HS}(r) = \begin{cases} \infty, & r < \sigma, \\ 0, & r \geqslant \sigma. \end{cases} \tag{22}$$

Monomers within the same chain have a fixed bond length of σ and are thus bonded tangentially. The only other constraint is the nonlocal hard sphere interaction between beads more than one segment apart, so that the chain is otherwise fully flexible. We will consider systems with slit pore geometry and a purely repulsive and athermal wall of the form

$$V_{wall}(z) = \begin{cases} \infty, & z < \sigma/2, \\ 0, & z \geqslant \sigma/2. \end{cases} \tag{23}$$

B. Liquid-Vapor Surface Tensions

1. Surface tension of the Lennard-Jones fluid

The methodology proposed was first explored and tested using the Lennard-Jones fluid, since several other methods have already been tested for this system. The interactions were truncated at $R_c=2.5\sigma$, with no further shift of the potential [this corresponds to the spherically truncated (ST) Lennard-Jones model of Trokhymchuk and Alejandre [14]]. The simulated boxes had an initial size of $13\times13\times45$, containing a total of 2137 particles. The production stage was organized in cycles. Each such cycle consisted of 2000 attempted canonical attempts to displace a particle. Half of these attempts were standard metropolis displacements set to yield about 50% acceptance. The remaining half consist of biased deletion-insertion movements [52]. First, a particle chosen at random was deleted. The particle was then inserted into one among several randomly chosen positions with a probability given by the corresponding Rosenbluth weights. The attempted displacement was accepted or rejected following the configurational bias rules [53]. It is expected that this trial move will accelerate the proper equilibration between the vapor and liquid phases and provide a better sampling of the interface than the metropolis movements alone. After the end of each cycle, a box deformation attempt was performed, with Δ_{att} set during the equilibration period to yield about 50% acceptance. Averages were collected over about 0.5×10^6 cycles to 1×10^6 cycles.

Before considering the performance of the method proposed in the previous section, with the specific bracketing choice for W [cf. Eq. (16)], it is interesting to consider the performance of an alternative countertension function selected so as to produce a proper equilibrium state. The surface tension will favor states such that γA is minimum. In order to equilibrate this contribution, an extra term acting in the opposite direction is needed. A possible choice that was considered is

$$W(A) = 2\xi A_0^2/A, \tag{24}$$

where $A_0=V^{2/3}$ is introduced in the equation so that the parameter ξ has the same dimensions as γ. At constant N, V, and T, the relevant Helmholtz free energy for the system in this case is simply

$$F(A) = 2\xi A_0^2/A + 2\gamma A. \tag{25}$$

Minimizing the free energy it is found that the equilibrium state of the surface area is such that

$$\frac{A}{A_0} = \left(\frac{\xi}{\gamma}\right)^{1/2}. \tag{26}$$

Therefore, the average interfacial area obtained from a simulation allows one to calculate the surface tension. An obvious way to test the above equation is by performing several simulations with different ξ values. A plot of $(A/A_0)^2$ against ξ will produce a straight line with slope γ. This test is shown in the inset of Fig. 1 for the ST-LJ model at $T=0.85\epsilon/k_B$. The plot clearly shows a straight line with slope $\beta\gamma=(0.779\pm0.010)\sigma^2$, in good agreement with the $\beta\gamma=(0.772\pm0.010)\sigma^2$ result suggested by Trokhymchuk and Alejandre from explicit evaluation of the virial [14]. In that figure, results obtained by the balance method for several other temperatures is also shown. Good agreement with Ref. [14] is found in most cases. A more detailed analysis of the results, together with the average surface area and ξ values employed, is reported in Table I. This is an important parameter, because γ is known to show a significant dependence on the lateral system size [54,55]. Our results were performed for similar system sizes as those reported in Ref. [14], and the comparison shows good agreement. The only large discrepancy is found for the relatively high temperature $T=1.127\epsilon/k_B$, close to the critical point. A reliable estimate of γ at such high temperature is difficult for several reasons. The interface width diverges close to the critical point, the bulk densities are attained only asymptotically slowly, and the results will depend also on the perpendicular length L_z and the length between the two interfaces as well. One advantage of the method proposed here is that the interface is allowed to fluctuate, so that the value of γ that is obtained is averaged out over a finite interval of lateral lengths. For high temperatures these fluctuations can be large. Indeed, the interfacial areas sampled during the simulation of the system at $T=1.127\epsilon/k_B$ for $\xi=0.0075\epsilon/\sigma^2$ fall broadly in an interval of lateral lengths between 10σ and 14σ. Unfortunately, these large fluctuations could actually be more a matter of concern than an advantage. For a very large system, the fluctuations about the equilibrium interface area will be Gaussian and the average interfacial area will be equal to the extremum of the distribution. For finite systems as in our simulations, the large fluctuations imply that the interface area is actually sampling a non-Gaussian-skewed distribution of the form $f(x)\sim\exp[-(ax+b/x)]$, with x the random variable and a and b some coefficients. In such a case, the average and the

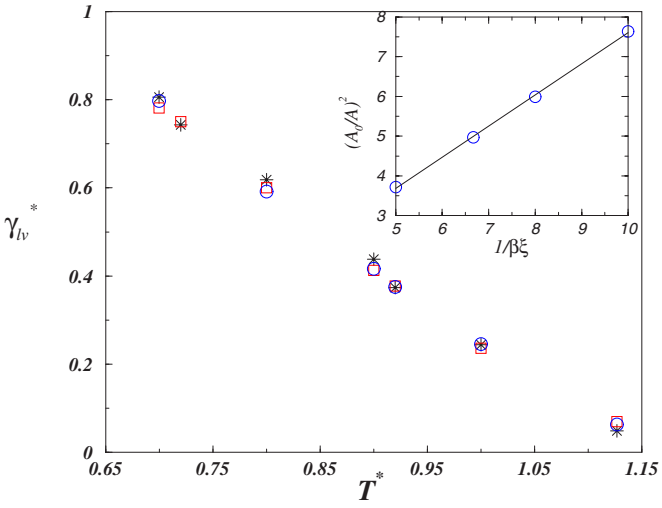

FIG. 1. (Color online) Liquid-vapor surface tension of the spherically truncated ($R_c=2.5$) Lennard-Jones model $\gamma^*=\gamma_{lv}\sigma^2/\epsilon$ as a function of temperature $T^*=k_BT/\epsilon$. The squares and circles are obtained from the contertension and the bracketed sampling methods, respectively. The stars are results from [14]. The inset is a plot of the inverse-squared surface area against $1/\beta\xi$, with slope equal to $\beta\gamma$.

TABLE I. Surface tension for the spherically truncated Lennard-Jones potential as determined by the wandering interface method with balance and bracket sampling. Results obtained from the virial method are also shown for comparison [14]. Range column includes βk for the countertension method or the surface range sampled for the bracket method. The size column indicates either the average lateral size for the wandering interface methods or the fixed lateral size for the virial method. Averages for balance sampling were collected over 400 kcycles, except for those indicated with an asterisk, collected over twice as many. Averages for the bracket sampling were collected over 1000 kcycles.

k_BT/ϵ	Method	Constraint	System size	$\sigma^2\gamma_{lv}/\epsilon$
0.70	balance	0.276	13.88	0.781(8)
0.70	bracket	[169, 181]	13.19	0.815(2)
0.70	bracket	[179, 183]	13.40	0.797(10)
0.70	virial		13.41	0.806(16)
0.72	balance	0.175	12.59	0.75(2)
0.72	bracket	[146, 158]	12.11	0.735(4)
0.72	virial		13.41	0.743(3)
0.80*	balance	0.200	14.16	0.594(5)
0.80*	balance	0.150	13.17	0.598(6)
0.80*	balance	0.125	12.57	0.601(6)
0.80	balance	0.100	11.83	0.61(2)
0.80	bracket	[179, 183]	13.40	0.591(7)
0.80	virial		13.41	0.618(9)
0.90*	balance	0.0756	12.54	0.413(3)
0.90	bracket	[178, 184]	13.38	0.416(9)
0.90	virial		13.41	0.438(4)
0.92	balance	0.0903	13.49	0.377(7)
0.92	bracket	[177, 185]	13.35	0.375(8)
0.92	virial		13.41	0.374(6)
1.00	balance	0.0466	13.14	0.236(6)
1.00	bracket	[172, 190]	13.19	0.246(5)
1.00	virial		13.41	0.244(5)
1.127*	bracket	[133, 139]	11.65	0.0637(8)
1.127	bracket	[170, 190]	13.29	0.0633(2)
1.127*	balance	0.0057	10.97	0.070(3)
1.127*	balance	0.0075	11.76	0.069(4)
1.127	virial		13.41	0.049(6)

extremum may deviate significantly, and Eq. (25) might not be a reliable estimate of the surface tension.

However, the most important problem with the counter tension methodology is in fact the choice of ξ. Note that the average surface area that resulted from our simulations is such that the lateral length remains close to the initial value $L=13\sigma$ for most temperatures (cf. Table I). Obviously, a look at Eq. (25) shows that this cannot be achieved accidentally. For an arbitrary choice of ξ, the resulting equilibrium geometry may produce problems. For any ξ larger than γ, it is clear that the average equilibrium surface is larger than A_0. As a result, the lateral length becomes larger than the perpendicular length and the system becomes metastable: i.e., the liquid slab will have tendency to rotate by $\pi/2$ so as to achieve a minimal surface area. For values of ξ that are too large, on the contrary, the simulation box will stretch very much and produce a long slab with very small surface area. The surface tension that is obtained will then strongly depend on the equilibrium state, while use of Eq. (25) which was derived by ignoring the system size dependence of γ could be again not adequate. Obviously, one can always choose ξ such that $\langle A\rangle$ falls within some desired range as was done in this work, but this implies a reasonable first guess of γ, which is not always at hand.

The bracketed interfacial area sampling proposed in the previous section overcomes all of these problems. First, the sampling interval may be set at will right away, avoiding visits to undesired regions. Second, no prior knowledge of γ is required. Table I shows the results obtained using the bracketing sampling strategy. Overall good agreement with both the virial and the balance sampling method is found, though the results for the near to critical temperature $T=1.127\epsilon/k_B$ are again in conflict with those obtained from the virial method. On the other hand, both methods employed in this work provide results in fair agreement for that temperature, given that the lateral system sizes studied differ considerably and the countertension method could suffer from the problems discussed above.

One important issue with the bracket sampling is the choice of bracketing interval $[A_{min},A_{max}]$. On the one hand, a large interval is difficult to explore, because the states with large surface area are exponentially suppressed and so will suffer from poor sampling. On the other hand, large Δy and Δx values will lead to a small relative error of the slope, $\Delta y/\Delta x$. Clearly, choosing the optimal value is not a trivial matter, although we expect the optimal choice will depend on the dimensionless parameter $\xi=2\beta\gamma\Delta A$. For $T=0.70\epsilon/k_B$ and $T=1.00\epsilon/k_B$ two set of simulations with different values of ξ were performed. In set S, a small interval was chosen, corresponding to a small expected ξ of about 1. On the contrary, in set L we chose $\xi\sim 9$ such that $f_{NVT}(A)$ varied about three orders of magnitude. The statistical analysis based on partial results of $2\beta\gamma$ obtained from Eq. (17) after averaging the surface over 500 000 cycles remains inconclusive. The error as measured from the standard deviation of the sample is very similar in both sets, and no significant differences in the mean are observed either. For the state point at $T=0.70\epsilon/k_B$ set S yields $2\beta\gamma=(2.245\pm0.050)\sigma^{-2}$ while two independent runs of set L produced $2\beta\gamma=(2.282\pm0.040)\sigma^{-2}$ and $2\beta\gamma=(2.277\pm0.027)\sigma^{-2}$. Similarly, for $T=1.00\epsilon/k_B$ set S produced $2\beta\gamma=(0.490\pm0.015)\sigma^{-2}$ while set L yields $2\beta\gamma=(0.498\pm0.017)\sigma^{-2}$ and $2\beta\gamma=(0.490\pm0.011)\sigma^{-2}$.

2. Surface tension of the square well fluid

Calculation of the surface tension from the anisotropy of the pressure tensor is particularly difficult for fluids with discontinuous potentials. In such cases, there appears a δ function Dirac in the virial expression for every discontinuity in the potential. In practice, this means that the instantaneous virial can only be measured approximately and that the computer program must be tailored for each model. The method

TABLE II. Surface tension for the square well fluid with $\lambda = 1.5\sigma$. Results from this work are compared with the virial method [5] and with the test area method [34].

k_BT/ϵ	Method	Constraint	System size	$\sigma^2\gamma_{lv}/\epsilon$
0.90	bracket	[173.75, 174.25]	13.19	0.431(40)
0.90	virial		10	0.423(10)
0.90	TAM		10.76	0.468(18)
0.95	bracket	[170.75, 171.25]	13.08	0.351(36)
0.95	virial		10	0.349(9)
0.95	TAM		10.88	0.336(20)
1.00	bracket	[170.7, 171.0]	13.07	0.256(20)
1.00	virial		10	0.268(13)
1.00	TAM		11.01	0.288(20)
1.05	bracket	[170.15, 170.45]	13.05	0.166(21)
1.05	virial		10	0.202(11)
1.05	TAM		11.18	0.205(14)
1.10	bracket	[168.75, 169.25]	13.00	0.132(22)
1.10	virial		10	0.142(12)
1.10	TAM		11.39	0.153(14)

of interface sampling has the advantage of not requiring explicit evaluation of the virial, and this may prove particularly advantageous in this case.

In this section the simple square well fluid with $\lambda = 1.5\sigma$ is chosen as a prototypical discontinuous model potential. Simulations were performed on systems containing overall 2222 atoms and initial system size of $13 \times 13 \times 45$. The sampling strategy is exactly the same as with the Lennard-Jones fluid, with cycles of 2222 center of mass and configurational bias moves in the ratio 50:50.

The difficulties in sampling the square well fluid interface are illustrated by considering the countertension method explained in the previous section. In order to achieve a reasonable acceptance rate for the box deformations, the maximal random displacement has to be set to very small values, and it becomes difficult for the system to reach a meaningful equilibrium value of the interface area. For a temperature of $T = 1.00\epsilon/k_B$ a value of $\Delta = 0.035\sigma^2$ was required to achieve the prescribed 50% acceptance ratio in box deformations. On the other hand, a value of $\Delta = 0.65\sigma^2$ was obtained for the Lennard-Jones fluid at the lowest temperature studied. Assuming a simple random walk for the interface displacements, this would imply that the square well fluid needs $(0.65/0.035)^2$ more cycles than the Lennard-Jones fluid in order to sample the same surface area. In these conditions, the countertension method becomes inefficient and the bracket sampling strategy with a small interval of about $0.5\sigma^2$ is more convenient. Even so, the simulations were performed over 10×10^6 cycles in order to achieve error bars comparable to those obtained for the Lennard-Jones fluid.

The results obtained using the bracket sampling are shown in Table II. Good agreement with previous results using the virial method, the test area method, and Binder's method is found [15,34,56].

In the test area method (TAM), a simulation is carried out in an *NVT* ensemble of fixed shape. Every cycle, a "test" deformation at constant volume is performed and the corresponding change in configurational energy, ΔU, is measured. Following Gloor *et al.*, it can be shown that the surface tension is given as

$$\gamma_{lv} = \lim_{\Delta A \to 0} -k_B T \frac{\ln \langle e^{-\beta \Delta U} \rangle_0}{\Delta A}, \tag{27}$$

where the subscript "0" denotes that the interface is sampled over the unperturbed system. In the limit where the method becomes exact, it becomes equivalent to measuring the anisotropy of the pressure tensor, with the virial evaluated numerically instead of analytically. Indeed, for small enough deformations, the instantaneous energy change may be written as

$$\Delta U(\{\mathbf{r}^N\}) = \left(\frac{\partial U(\{\mathbf{r}^N\})}{\partial A} \right)_V \Delta A. \tag{28}$$

Accordingly, an asymptotically exact Taylor expansion of Eq. (27) yields right away:

$$\gamma_{lv} = \left\langle \left(\frac{\partial U(\{\mathbf{r}^N\})}{\partial A} \right)_V \right\rangle_0. \tag{29}$$

From the canonical partition function one can show that the analytical derivative in this equation is just the anisotropy of the pressure tensor. Both the TAM and the interface sampling proposed in this work have the advantage of avoiding the explicit calculation of the virial. However, the interface sampling method could avoid difficulties encountered with the TAM due to the nonequivalence between compressing and expanding the interface in discontinuous systems [34]. For very small deformations the three methods should become equivalent, although the virial method would seem to yield results with smaller error bars [35].

C. Fluid-Substrate Interfacial Tensions

1. Interfacial tensions of Lennard-Jones chains

In this section the interfacial tensions of the bead-spring polymer model described at the beginning of this section are considered. The interfacial properties of chains with ten beads at a subcritical temperature of $T = 1.68\epsilon/k_B$ have been studied previously and are well known [9,17]. The liquid-vapor surface tension has been calculated using Binder's method, while the spreading coefficients $\gamma_{wv} - \gamma_{wl}$ were also evaluated with a related method all the way from the wetting to the drying transition [9]. The interfacial tensions of the glassy polymer in narrow slit pores have also been measured using the virial method [17].

Simulations for the polymer model were carried out in the grand canonical ensemble (see Fig. 2). The chemical potential was fixed to its coexistence value, and the initial box size was set to $13.8 \times 13.8 \times 27.6$ (i.e., for the liquid state, this amounts to about 315 polymers in the simulation box). The configurational space was sampled by means of center-of-mass displacements, standard canonical configurational bias displacements, and grand canonical configurational bias insertion and deletion attempts in the ratio 25:25:50. For the

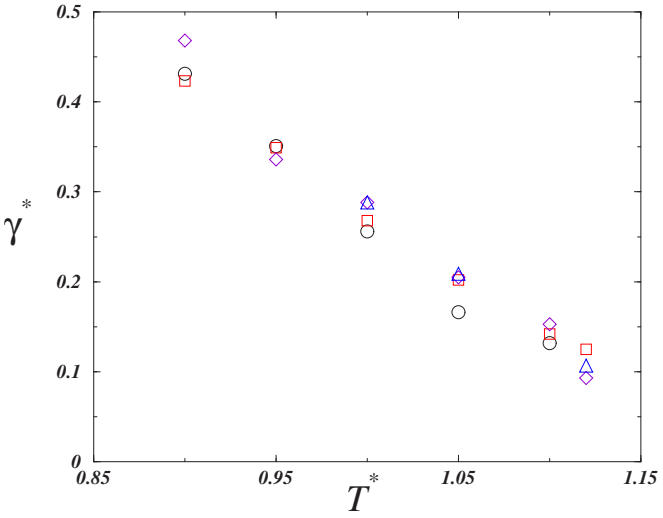

FIG. 2. (Color online) Liquid-vapor surface tension of a square well fluid with $\lambda=1.5\sigma$. Results are given in reduced units, with $\gamma^*=\gamma_{lv}\sigma^2/\epsilon$ plotted as a function of temperature $T^*=k_BT/\epsilon$. Circles: results from the bracketed sampling method of this work. Squares: anisotropy of the virial tensor [15]. Diamonds: test area method [34]. Triangles: Binder's method [56].

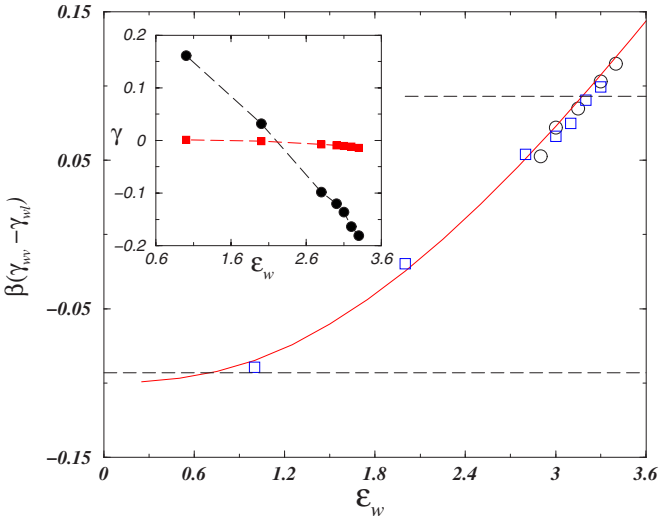

FIG. 3. (Color online) Wall-fluid interface tensions for the LJ-FENE model. The figure shows the spreading coefficient $\gamma_{wv}-\gamma_{wl}$ as a function of wall strength ϵ_w. Squares are results obtained in this work from explicit evaluation of γ_{wv} and γ_{wl}. Circles and lines are results for the spreading coefficients from Ref. [9]. The dashed horizontal lines correspond $\pm\gamma_{lv}$ and the intersections correspond to wetting and drying transitions. The inset shows the tensions as a function of wall strength. Circles and squares refer to the wall-liquid and wall-vapor tensions, respectively.

vapor phase only the last two kinds of trial moves were attempted. The maximum allowed box deformation attempts were adjusted during the equilibration period as to provide roughly a 50% acceptance ratio. Averages were collected over roughly 1.5×10^6 cycles for wall-liquid tensions and about 5×10^6 cycles for the wall-vapor tensions.

The results obtained for both the wall-liquid and wall-vapor interface tensions may be found in Table III. Also included are the differences $\gamma_{wv}-\gamma_{wl}$ previously calculated using two different methods. The comparison shows excellent agreement for the spreading coefficient and thus provides strong support for the methodology. The liquid-vapor surface tension was also calculated using the interface sampling in the canonical ensemble with a $13.5\times13.5\times50$ box geometry and 185 molecules. The result $\gamma_{lv}=(0.156\pm0.008)\epsilon/\sigma^2$ is in good agreement with previous measurements using Binder's method, $\gamma_{lv}=0.160\epsilon/\sigma^2$ [9].

For many practical applications, the relevant property is not really the surface tensions alone, but the corresponding spreading coefficient, which governs both the wetting behavior of a single interface and the capillary condensation-evaporation phenomenology. Figure 3 shows the results of the spreading coefficient as a function of ϵ_w. The points where the spreading coefficient crosses the liquid-vapor surface tensions indicate the location of wetting-drying transitions. Independent measurement of the tensions remains interesting, because it allows one to compare the free energy of the wall-fluid interface relative to that of a bulk system of equal volume. Such data are useful for comparison with self-consistent and density functional theories, but can be also relevant in processes were the interface is free to grow—i.e., nucleation or self-assembly of biological systems. Table III shows that both γ_{wv} and γ_{wl} are negative for strongly attractive walls but change sign as the effective Hamaker constant decreases. For positive but small values of ϵ_w the weak attractive interactions are not able to compensate for the free energy cost of a inhomogeneous density profile. The fact that the liquid phase requires a wall strength larger than $\epsilon_w=2\epsilon$ before it becomes negative is consistent with previously observed density profiles, which remain considerably depleted for ϵ_w as large as 3ϵ and only start to develop monomerlike oscillatory behavior at about that value. Actually, γ_{wl} is about one order of magnitude larger than γ_{wv} all the way from $\epsilon_w=0$ to $\epsilon_w=3.30$ and dominates completely the behavior of $\gamma_{wv}-\gamma_{wl}$. At $\epsilon_w=0$ both the wall-vapor and wall-liquid interfaces are unfavorable relative to the corresponding bulk phases and the drying transition is actually driven by the very unfavorable wall-liquid interface.

TABLE III. Wall-fluid interface tension for a bead-spring polymer model (FENE-LJ) at $T=1.68$. Interface tensions are given in units of the Lennard-Jones energy parameter ϵ.

ϵ_w	γ_{wl}	γ_{wv}
3.30	−0.181(6)	−0.0139(3)
3.20	−0.164(12)	−0.0119(3)
3.10	−0.136(15)	−0.0106(3)
3.00	−0.120(10)	−0.0095(6)
2.80	−0.098(7)	−0.0072(1)
2.00	0.032(8)	−0.0015(1)
1.00	0.161(10)	0.0011(2)
0.00		−0.00009(10)

TABLE IV. Chemical potentials (μ/k_BT) of tangent hard sphere chains for several chain lengths m and monomer densities ρ. The results for $m=12$ and $m=16$ at $\rho=0.60\sigma^{-3}$ could not be measured from the NVT+test particle method and merely correspond to the chemical potential imposed during the simulations. Results for μ/k_BT are given as an excess over ideal chains. The entry for zero density is the difference between real and ideal chain contributions (see Ref. [71] for a discussion on reference states appropriate to configurational bias grand canonical simulations).

ρ/m	2	4	8	12	16
0.00	0	0.6277	2.1085	3.6495	5.2118
0.10	−2.34814(4)	−2.12764(7)	−0.8409(1)	0.7589(2)	2.4841(2)
0.20	−0.81907(5)	−0.1513(1)	1.9751(2)	4.3995(6)	6.9482(8)
0.30	0.67658(5)	2.0178(3)	5.4555(4)	9.19(2)	13.060(2)
0.40	2.4000(2)	4.7275(3)	10.123(2)	15.81(7)	21.59(7)
0.50	4.5358(6)	8.296(2)	16.5(1)	25.19(3)	34(2)
0.60	7.308(1)	13.126(5)	25.2(4)	43	54

2. *Interfacial tensions of chains of tangent hard spheres at an athermal wall*

Having studied the performance of the method for fluids with discontinuous potentials (square well) and for polymer chains (FENE-LJ), we now consider a fluid made of tangent hard sphere chains adsorbed on purely repulsive athermal walls. This system has been the subject of great interest in the last decade, as a prototypical model for the study of polymer-wall interfaces, as well as a test bead for density functional theories [24,57,58].

We have considered chains of 2, 4, 8, 12, and 16 monomers adsorbed on a hard wall. For each chain, we have calculated the interface tensions corresponding to six different bulk densities of approximately 0.1, 0.2, 0.3, 0.4, 0.5, and 0.6 monomers per σ^3. We first performed bulk NVT simulations for those densities and evaluated the chemical potential by means of Widom's test particle method. For the largest chains at high density, Widom's test failed and the grand potential could not be properly evaluated. An arbitrary value was imposed in those cases, based on the approximation that the excess chemical potential is linear in the chain length. The values of the chemical potentials employed in the simulations are collected in Table IV. Once the desired chemical potential was known, grand canonical simulations were performed on a system with initial size of $15\times15\times35$. The grand canonical distribution function was sampled by using center-of-mass, rotation, configurational bias, and grand canonical configurational bias insertion and deletion moves in the ratio 15:15:35:35, except for dimers, where the ratio was set to 15:15:0:70. After suitable equilibration, averages were collected over $3-7\times10^6$ cycles, with longer runs required for the highest densities.

The choice of bracketing interval in this case is also a matter of concern, since the conditions change over a wide interval and the trial displacements required to achieve 50% acceptance in the box shape moves vary from about $3\sigma^2$ to about $3\times10^{-2}\sigma^2$ as the monomer density increases from $0.1\sigma^{-3}$ to $0.6\sigma^{-3}$ (this parameter being much less sensitive to chain length). At this stage we developed a systematic method to decide the size of the lateral size sampling interval which works well. A short simulation of about 100 000 cycles is performed, and the lateral-size mean-squared displacement is calculated. A plot as a function of Monte Carlo (MC) cycles shows an initial linear and steady growth corresponding to the unconstrained diffusion process, followed by a plateau occasioned by the reflecting boundary conditions on the lateral size (Fig. 4). Measuring an effective diffusion coefficient D_{eff} from the slope of the mean-squared displacement within the first regime allows us to estimate the expected lateral-size displacement within a given number of cycles. Obviously, the lateral size needs to have reflected several many times if meaningful averages are to be collected. Therefore, the size of the sampling interval required for the condition to be obeyed within a prescribed amount n_{block} of MC cycles may be estimated from D_{eff}. In practice, we chose the sampling interval from the distance traveled during 10000 cycles.

The results of our calculations are presented in Table V. As seen from the table, the surface tensions could be evaluated with relative errors lying between 1% and 10%, with

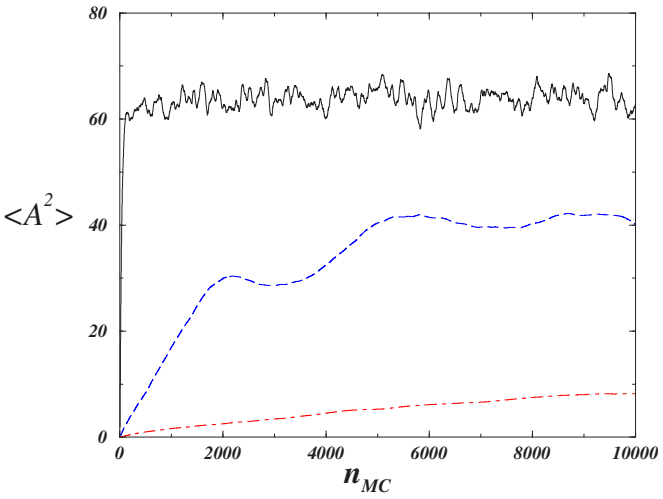

FIG. 4. (Color online) Surface-area mean-squared displacement as a function of Monte Carlo cycles for chains of length $m=16$. From top to bottom, results refer to monomer densities $\rho=0.10\sigma^{-3}$ (solid line), $\rho=0.30\sigma^{-3}$ (dashed line, 2 times magnified), and $\rho=0.50\sigma^{-3}$ (dash-dotted line, 10 times magnified).

TABLE V. Wall-fluid interface tension for tangent hard sphere chains on athermal substrates for several chain lengths m and monomer densities ρ (cf. Table IV for chemical potentials). The entries of the table are interface tensions γ/k_BT. Results are given in units of the hard sphere diameter.

ρ	2	4	8	12	16
0.10	0.0447(5)	0.0352(4)	0.0295(4)	0.0273(4)	0.0248(2)
0.20	0.104(2)	0.0905(10)	0.0788(14)	0.0755(10)	0.0745(14)
0.30	0.197(6)	0.159(6)	0.148(4)	0.149(5)	0.153(3)
0.40	0.347(15)	0.278(11)	0.26(9)	0.240(7)	0.25(2)
0.50	0.44(3)	0.43(2)	0.40(3)	0.375(11)	0.40(2)
0.60	0.83(8)	0.63(3)	0.60(4)	0.61(5)	0.52(4)

accuracy deteriorating at the highest densities. Inspection of the results as plotted in Fig. 5 shows that the interface tensions are always positive, increase with monomer density, and decrease with chain length. Simulation results suggest an asymptotic behavior for long chains at low densities. For higher densities, however, the error bars are too large and this trend cannot be confirmed.

Hooper *et al.* have calculated the interface tensions of athermal chains with no intramolecular excluded-volume interactions [24]. These authors find that the interface tension of a 20-mer first increases with density, but then gradually decreases and actually becomes negative at high densities. The different behavior is related to the choice of dividing surface [cf. Eq. (23)]. In this work the dividing surface coincides with the actual wall surface (i.e., $z=0$), while Hooper *et al.* assume that the dividing surface is located at the distance of the closest approach of a segment to the surface (i.e., $z=\sigma/2$). Our results can be easily recalculated to another choice of the dividing surface by using the simple relation $\gamma_{z=\sigma/2}=\gamma_{z=0}-\frac{1}{2}p\sigma$, where the subscripts stand for the location of the dividing surface and p is the bulk pressure [cf. Eq. (4.3) in Ref. [24]]. This equation shows that our choice of dividing surface yields what is sometimes known as the intermolecular contribution to the interfacial tension. For the proposed method, the choice of dividing surface is implied in the volume definition [35]. Here we have employed $V=A\times L_z$, while restricting the system's volume to that space available to the molecule's center of mass we would require $V=A\times(L_z-\sigma)$ (a slit pore is used in practice, so $\frac{1}{2}\sigma$ must be subtracted twice). These definitions dictate the length-to-breadth ratio of attempted deformations in the Monte Carlo simulation and thus produce interfacial tensions according to the choice of dividing surface. In order to illustrate this point, we have performed some simulations for chains of length $m=12$ and a dividing surface located at $z=\sigma/2$. Figure 6 presents a plot of the simulation results, clearly showing the nonmonotomic trend observed by Hooper *et al.* [24]. Included as squared symbols are results for $\gamma_{z=\sigma/2}$ obtained from our previously calculated $\gamma_{z=0}$ and shifted by $-\frac{1}{2}p\sigma$. The results agree within the error interval.

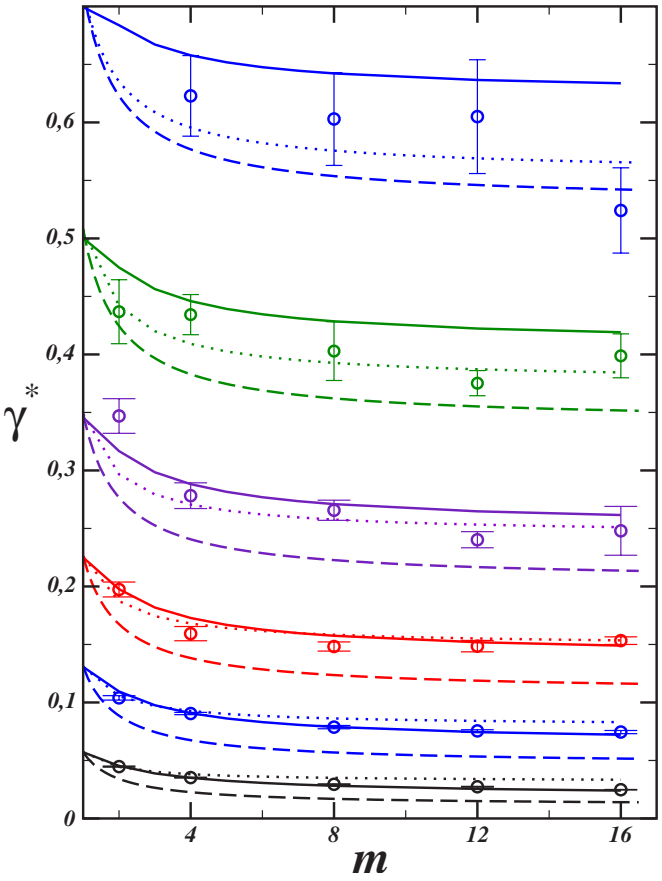

FIG. 5. (Color online) Wall-fluid interface tensions for hard sphere chains adsorbed on an athermal substrate as a function of chain length. From top to bottom, results refer to $\rho=0.1\sigma^{-3}$, $\rho=0.2\sigma^{-3}$, $\rho=0.3\sigma^{-3}$, $\rho=0.4\sigma^{-3}$, $\rho=0.5\sigma^{-3}$, and $\rho=0.6\sigma^{-3}$. Symbols show simulation results from this work. Lines are theoretical results: Solid line, TPT1-DFT; dashed line, SPT; dotted lines, DFT-based analytical approximation.

Along with the simulation results, we also include predictions from three different theoretical treatments. The first approach is based on scaled particle theory (SPT) [29], which has been shown to be accurate for fluids of spherical symmetry, whether hard spheres [35,59] or Lennard-Jones fluid [60]. In this approach one considers the free energy change that results from inserting a large particle and identifies the chemical potential with macroscopic contributions arising from pV and surface work [30,60,61]:

$$d\mu_\sigma = 2\pi\gamma\sigma d\sigma + \frac{\pi}{2}p\sigma^2 d\sigma, \tag{30}$$

where μ_σ denotes the chemical potential of the large particle of diameter σ inserted in the fluid. The macroscopic interface

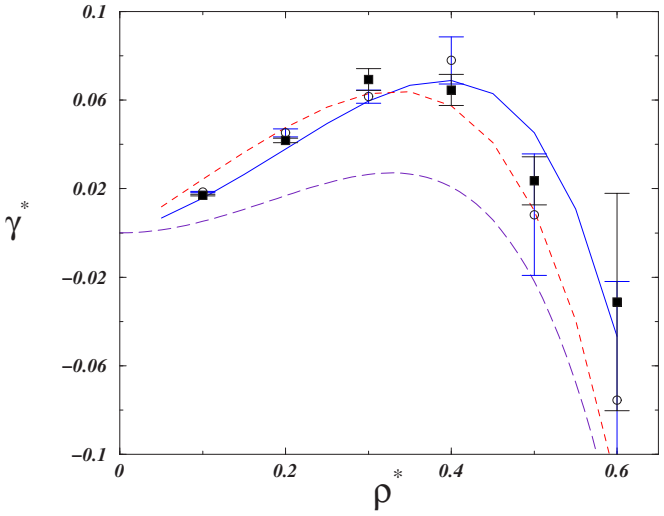

FIG. 6. (Color online) Wall-fluid interface tensions for hard sphere chains of length $m=12$ adsorbed on an athermal substrate with the dividing surface located at $z=\frac{1}{2}\sigma$. The circles are simulation results with the volume of the slit pore defined as $V=(L_z-\sigma)$. The solid squares are results obtained by subtracting $\frac{1}{2}p\sigma$ from the simulated data for $\gamma_{z=0}$. The lines are theoretical results. Solid line, TPT1-DFT; dashed line, SPT; dotted lines, DFT-based analytical approximation.

tension for a flat interface is obtained from the above equation in the limit of infinite dilution and particle diameter as a term proportional to σ. Here we consider a fluid mixture of tangent hard sphere chains and large hard sphere particles as described by Wertheim's perturbation theory [45], together with the Boublik equation of state for the hard sphere reference mixture [62]. After some tedious algebra, we obtain

$$\pi\beta\sigma^2\gamma = \frac{1}{(1+\eta)^2(1-\eta)^2}\{(3-6\eta^2+3\eta^4)\ln(1-\eta) + 3\eta + 14\eta^2 - 5\eta^4 - \eta^5 + \eta^6 + (3\eta - 5\eta^2 + 2\eta^4 + \eta^5 - \eta^6)/m\}. \quad (31)$$

The second approach is based on microscopic density functional theory for polymeric fluids [8,43,44]. Within this framework the grand potential of the system is a functional of the local density of polymer $\rho(\mathbf{R})$,

$$\Omega[\rho(\mathbf{R})] = \int d\mathbf{R}\rho(\mathbf{R})[V_{ext}(\mathbf{R}) - \mu] + \beta^{-1}\int d\mathbf{R}\rho(\mathbf{R})\{\ln[\rho(\mathbf{R})] - 1\} + \int d\mathbf{R}V_b(\mathbf{R})\rho(\mathbf{R}) + F_{ex}[\rho_{PS}(\mathbf{r})]. \quad (32)$$

In the above $\mathbf{R}=(\mathbf{r}_1,\mathbf{r}_2,\ldots,\mathbf{r}_m)$ denotes the set of segment positions and V_{ext} is the external potential, while V_b is the bonding potential that satisfies $\exp[-\beta V_b(\mathbf{R})]=\Pi_{i=1}^{m-1}[\delta(|\mathbf{r}_{i+1}-\mathbf{r}_i|-\sigma)]/(4\pi\sigma^2)$. $F_{ex}[\rho_{PS}(\mathbf{r})]$ is the excess free energy approximated as a functional of the average segment density defined as $\rho_{PS}(\mathbf{r})=\Sigma_{i=1}^{m}\int d\mathbf{R}\,\delta(\mathbf{r}-\mathbf{r}_i)\rho(\mathbf{R})$. In this work we apply the Yu-Wu functional for F_{ex}, which is based on the fundamental measure theory of Rosenfeld [43,63]. According to this approach the excess free energy is a volume integral $\beta F_{ex}=\int d\mathbf{r}\Phi$. The excess free energy density Φ is a simple function of a set of weighted densities $\{n_\alpha\}$, $\alpha=3,2,1,0,V1,V2$, defined as

$$n_\alpha(\mathbf{r}) = \int d\mathbf{r}'\rho_{PS}(\mathbf{r}')w_\alpha(\mathbf{r}-\mathbf{r}'). \quad (33)$$

The weight functions w_α depend on geometrical properties of the segments and are given explicitly in Refs. [43,63].

In the Yu-Wu theory the excess free energy density is represented as a sum of two contributions, $\Phi=\Phi_{HS}+\Phi_P$. Φ_{HS} describes the reference mixture of hard spheres and is based on the Boublik equation of state [62,64,65]

$$\Phi_{HS} = -n_0\ln(1-n_3) + \frac{n_1n_2-\mathbf{n}_{V1}\cdot\mathbf{n}_{V2}}{1-n_3} + (n_2^3 - 3n_2\mathbf{n}_{V2}\cdot\mathbf{n}_{V2})\frac{n_3+(1-n_3)^2\ln(1-n_3)}{36\pi(n_3)^2(1-n_3)^2}, \quad (34)$$

while the excess free energy density due to the chain connectivity Φ_P is an "inhomogeneous counterpart" of the perturbation term in TPT1:

$$\Phi_P = \frac{1-m}{m}n_0\zeta\ln[y_{HS}], \quad (35)$$

where $\zeta=1-\mathbf{n}_{V2}\cdot\mathbf{n}_{V2}/(n_2)^2$. y_{HS} is the expression for the contact value of the hard sphere radial distribution function

$$y_{HS} = \frac{1}{1-n_3} + \frac{n_2\sigma\zeta}{4(1-n_3)^2} + \frac{(n_2\sigma)^2\zeta}{72(1-n_3)^3}. \quad (36)$$

The functional outlined above can be minimized numerically using the variational principle $\delta\Omega/\delta\rho(\mathbf{R})=0$. The resulting equilibrium density profile can be inserted into Eq. (32), yielding the grand potential which can be used to calculate the interfacial tension.

The third theoretical approach utilizes the bulk limit of the microscopic density functional theory outlined above. The starting point is the same homogenous one-component polymeric fluid as in the SPT route, and again we consider the change of the grand potential, $\beta\Delta\Omega$, due to the insertion of a single large hard sphere into the system. This change can be expressed in terms of the derivatives of the excess free energy density:

$$\beta\Delta\Omega = \frac{\partial\Phi}{\partial n_3}\zeta_3 + \frac{\partial\Phi}{\partial n_2}\zeta_2 + \frac{\partial\Phi}{\partial n_1}\zeta_1 + \frac{\partial\Phi}{\partial n_0}\zeta_0, \quad (37)$$

where ζ_i, $i=3,2,1,0$, are characteristic functions of the shape of the inserted large particle [31,66,67]. In particular ζ_3 and ζ_2 are, respectively, the volume and the area of the large inserted hard sphere. If the functional was fully consistent with the SPT theory, the volume-dependent term $\partial\Phi/\partial n_3$ should give the pressure, while the area-dependent term $\partial\Phi/\partial n_2$ should give the planar wall-fluid interfacial tension ($\partial\Phi/\partial n_1$ and $\partial\Phi/\partial n_0$ should give the curvature-dependent corrections to the surface tension [31,66,67]). The functional

given by Eqs. (34)–(36) is not fully consistent with SPT but accepting this deficiency we can still identify the area-dependent term with the planar wall-fluid surface tension. Noting that in the bulk limit the vector weighted densities $\mathbf{n}_{V2}$ and $\mathbf{n}_{V1}$ vanish and $n_3 \to \eta$, $n_2 \to 6\eta/\sigma$ and $n_1 \to 3\eta/\sigma^2\pi$, $n_0 \to 6\eta/\sigma^3\pi$, the interfacial tension for tangent hard-sphere-polymer fluid at a hard wall is given as

$$\pi\beta\sigma^2\gamma = \pi\sigma^2\frac{\partial\Phi}{\partial n_2} = \frac{3\eta(2-\eta)}{(1-\eta)^2} + 3\ln(1-\eta) + \frac{1-m}{m}\frac{2\eta(3-\eta)}{(4-2\eta)}. \quad (38)$$

The first two terms on the right-hand side of Eq. (38) represent the interface tension for the hard sphere fluid at a hard wall and is the same as in the SPT approach presented above. The last contribution arises due to the chain connectivity but it differs from that of the SPT approach. Figure 5 presents the results for the interfacial tension of tangent hard sphere chains at a hard wall as a function of the chain length m. The sets of curves were calculated for the bulk segment densities ρ_σ^3=0.1, 0.2, 0.3, 0.4, 0.5, and 0.6 (from bottom to top, respectively). The circles denote the interface sampling simulation data. The solid lines are the results obtained by numerical minimization of the DFT, while the dashed and dotted lines denote, respectively, the SPT approach [Eq. (31)] and the DFT-based analytical approximation [Eq. (38)]. We note that the DFT results are in overall good agreement with simulations. The SPT approach always underestimates the interface tension, and the agreement is only qualitative. The DFT-based analytical approximation gives poor results at low density but it significantly improves at higher density. Note that, as mentioned earlier, the interface tension is always positive because the dividing surface is set at the actual wall surface. This choice is particularly useful for the theoretical treatment, since adding the $-\frac{1}{2}p\sigma$ extra contribution consistent with the choice of dividing surface at $z=\frac{1}{2}\sigma$ would obviously yield a less tractable equation. Figure 6 shows results for the interface tensions that result from this definition for chains of length m=12. Consistent with our previous observations, all three theoretical treatments provide qualitative agreement with simulations, though the Yu-Wu DFT theory and the corresponding DFT-based analytical approximation are in better agreement than the SPT approach.

V. CONCLUSIONS

We have developed a method for the efficient calculation of interface tensions by means of computer simulations. The method allows the interfacial area to wander randomly and extracts the interface tension from the resulting probability distribution. This strategy shares common features with Binder's method and perturbative methods such as those proposed by Bresme and Quirke and Gloor *et al.* [20,33,34]. On the one hand, it relies on histogram analysis or the related average of a sampled probability distribution; on the other hand, the sampling is the result of small finite deformations of the simulation box. The method avoids the explicit calculation of the pressure tensor and is therefore of great generality. It can be applied likewise for simple or complex fluids with continuous or discontinuous potentials and may be employed for interface tension calculations of free or bound interfaces. Any sampling method for the grand canonical or canonical distributions is appropriate, and improved sampling over wide ranges of box shape could be implemented using known techniques such as multicanonical [68], successive sampling [69], transition matrix [70], or Wang-Landau sampling [51].

The proposed method was tested for the Lennard-Jones and square well fluids, and good agreement was obtained with results found in the literature for similar system sizes. For systems with continuous potential, our results show that the method yields similar error bars at the same computational cost. The method runs into problems when the surface area cannot be sampled efficiently over a large interval. This is the case for the square well fluid, where somewhat greater error bars were found compared to the virial method at similar computational cost. On the other hand, the method is advantageous for the calculation of wall-substrate interfacial tensions at low density. In such cases, a large surface area can be sampled easily and low error bars result. In such cases, calculation of the interface tension via the pressure tensor anisotropy is a problem, because the small number of collision events prevents accurate estimation of the virial.

The technique was applied to the calculation of wall-fluid interfacial tensions for a bead-spring Lennard-Jones chain, providing results for both the wall-vapor and wall-liquid tensions. The related spreading coefficient was found to be in good agreement with previous results [9]. We also studied a system of tangent hard sphere chains adsorbed on athermal walls for a wide range of chain lengths and densities. At constant monomer density the interface tension approaches an asymptotic constant value from above. For constant chain length, the interface tension increases regularly with density. The results where used to test three different theories. Density functional theory as proposed by Yu and Wu [43], an analytical approximation based on that theory, and another analytic result inspired on scaled particle theory [29]. The latter approach reproduces the known accuracy for monomers, but deteriorates significantly with increasing chain length. On the other hand, the first two approaches provide rather good agreement. Particularly, the analytical result of Eq. (38) is surprisingly simple and yields predictions of similar good quality for all chain lengths studied.

ACKNOWLEDGMENTS

L.G.M wishes to thank Marcus Müller, F. J. Blas, E. de Miguel, F. Bresme, and C. Vega for helpful discussions; This work was supported by Ministerio de Educacion y Ciencia through a Ramon y Cajal grant and Project No. FIS200766079-C02-00 and by Comunidad Autonoma de Madrid through Project No. MOSSNOHO-S0505/ESP/0299. P.B. acknowledges the EU for partial funding this work as a TOK Contract No. 509249.

[1] J. Rowlinson and B. Widom, *Molecular Theory of Capillarity* (Clarendon, Oxford, 1982).
[2] R. Seemann, M. Brinkmann, E. J. Kramer, F. F. Lange, and R. Lipowsky, Proc. Natl. Acad. Sci. U.S.A. **102**, 1848 (2005).
[3] A. Milchev, M. Muller, and K. Binder, Phys. Rev. E **72**, 031603 (2005).
[4] L. G. MacDowell and M. Müller, J. Chem. Phys. **124**, 084907 (2006).
[5] J. S. Rowlinson, J. Stat. Phys. **20**, 197 (1979).
[6] J. W. Cahn and J. E. Hilliard, J. Chem. Phys. **28**, 258 (1958).
[7] P. Tarazona, Mol. Phys. **52**, 81 (1984).
[8] C. E. Woodward, J. Chem. Phys. **94**, 3183 (1990).
[9] M. Müller and L. G. MacDowell, Macromolecules **33**, 3902 (2000).
[10] P. Bryk and S. Sokolowski, J. Chem. Phys. **121**, 11314 (2004).
[11] P. Bryk, K. Bucior, S. Sokolowski, and G. Zukocinski, J. Phys.: Condens. Matter **16**, 8861 (2004).
[12] J. H. Irving and J. G. Kirkwood, J. Chem. Phys. **18**, 17 (1950).
[13] J. J. Magda, M. Tirrell, and H. T. Davis, J. Chem. Phys. **83**, 1888 (1985).
[14] A. Trokhymchuk and J. Alejandre, J. Chem. Phys. **111**, 8510 (1999).
[15] P. Orea, Y. Duda, and J. Alejandre, J. Chem. Phys. **118**, 5635 (2003).
[16] E. Martin del Rio and E. de Miguel, Phys. Rev. E **55**, 2916 (1997).
[17] F. Varnik, J. Baschnagel, and K. Binder, J. Chem. Phys. **113**, 4444 (2000).
[18] A. Milchev and K. Binder, J. Chem. Phys. **114**, 8610 (2001).
[19] D. Duque, J. C. Pamies, and L. F. Vega, J. Chem. Phys. **121**, 11395 (2004).
[20] K. Binder, Phys. Rev. A **25**, 1699 (1982).
[21] J. J. Potoff and A. Z. Panagiotopoulos, J. Chem. Phys. **112**, 6411 (2000).
[22] J. R. Errington, Phys. Rev. E **67**, 012102 (2003).
[23] L. G. MacDowell, J. Chem. Phys. **119**, 453 (2003).
[24] J. B. Hooper, J. D. McCoy, J. G. Curro, and F. van Swol, J. Chem. Phys. **113**, 2021 (2000).
[25] H. Furukawa and K. Binder, Phys. Rev. A **26**, 556 (1982).
[26] L. G. MacDowell, P. Virnau, M. Müller, and K. Binder, J. Chem. Phys. **120**, 5293 (2004).
[27] M. Müller and M. Schick, J. Chem. Phys. **105**, 8282 (1996).
[28] E. Chacon and P. Tarazona, J. Phys.: Condens. Matter **17**, S3493 (2005).
[29] H. Reiss, H. L. Frisch, and J. L. Lebowitz, J. Chem. Phys. **31**, 369 (1959).
[30] J. R. Henderson, Mol. Phys. **50**, 741 (1983).
[31] P. Bryk, R. Roth, K. R. Mecke, and S. Dietrich, Phys. Rev. E **68**, 031602 (2003).
[32] F. Bresme and N. Quirke, Phys. Rev. Lett. **80**, 3791 (1998).
[33] F. Bresme and N. Quirke, J. Chem. Phys. **110**, 3536 (1999).
[34] G. J. Gloor, G. Jackson, F. J. Blas, and E. de Miguel, J. Chem. Phys. **123**, 134703 (2005).
[35] E. de Miguel and G. Jackson, Mol. Phys. **104**, 3717 (2006).
[36] H. L. Vörtler and W. R. Smith, J. Chem. Phys. **112**, 5168 (2000).
[37] B. Widom, J. Chem. Phys. **39**, 2808 (1963).
[38] D. Chandler, J. D. McCoy, and S. J. Singer, J. Chem. Phys. **85**, 5971 (1986).
[39] E. Helfand, J. Chem. Phys. **56**, 3592 (1972).
[40] M. Müller and L. G. MacDowell, J. Phys.: Condens. Matter **15**, R609 (2003).
[41] A. L. Frischknecht, J. D. Weinhold, A. G. Salinger, J. G. Curro, L. J. D. Frink, and J. D. McCoy, J. Chem. Phys. **117**, 10385 (2002).
[42] J. B. Hooper, J. D. McCoy, and J. G. Curro, J. Chem. Phys. **112**, 3090 (2000).
[43] Y. X. Yu and J. Z. Wu, J. Chem. Phys. **117**, 2368 (2002).
[44] E. Kierlik and M. L. Rosinberg, J. Chem. Phys. **99**, 3950 (1993).
[45] M. S. Wertheim, J. Chem. Phys. **87**, 7323 (1987).
[46] R. Evans and U. M. B. Marconi, J. Chem. Phys. **86**, 7138 (1987).
[47] J. E. Finn and P. A. Monson, Phys. Rev. A **39**, 6402 (1989).
[48] J. E. Finn and P. A. Monson, Mol. Phys. **65**, 1345 (1988).
[49] J. Forsman and C. E. Woodward, Mol. Phys. **90**, 637 (1997).
[50] N. G. Almarza, E. de Miguel, and G. Jackson (private communication).
[51] F. G. Wang and D. P. Landau, Phys. Rev. Lett. **86**, 2050 (2001).
[52] L. G. MacDowell, C. Vega, and E. Sanz, J. Chem. Phys. **115**, 6220 (2001).
[53] J. I. Siepmann and D. Frenkel, Mol. Phys. **75**, 59 (1992).
[54] L.-J. Chen, J. Chem. Phys. **103**, 10214 (1995).
[55] P. Orea, Y. Duda, and J. Alejandre, J. Chem. Phys. **123**, 114702 (2005).
[56] J. K. Singh, D. A. Kofke, and J. R. Errington, J. Chem. Phys. **119**, 3405 (2003).
[57] R. Dickman and C. K. Hall, J. Chem. Phys. **89**, 3168 (1988).
[58] A. Yethiraj and C. E. Woodward, J. Chem. Phys. **102**, 5499 (1995).
[59] M. Heni and H. Löwen, Phys. Rev. E **60**, 7057 (1999).
[60] F. Bresme, J. Phys. Chem. B **106**, 7852 (2002).
[61] H. Reiss, H. L. F. E. Helfand, and J. L. Lebowitz, J. Chem. Phys. **32**, 119 (1960).
[62] T. Boublik, J. Chem. Phys. **53**, 471 (1970).
[63] Y. Rosenfeld, Phys. Rev. Lett. **63**, 980 (1989).
[64] R. Roth, R. Evans, A. Lang, and G. Kahl, J. Phys.: Condens. Matter **14**, 12063 (2002).
[65] Y. X. Yu and J. Z. Wu, J. Chem. Phys. **117**, 10156 (2002).
[66] P. M. König, R. Roth, and K. R. Mecke, Phys. Rev. Lett. **93**, 160601 (2004).
[67] H. Hansen-Goos and R. Roth, J. Phys.: Condens. Matter **18**, 8413 (2006).
[68] B. A. Berg and T. Neuhaus, Phys. Rev. Lett. **68**, 9 (1992).
[69] P. Virnau and M. Müller, J. Chem. Phys. **120**, 10925 (2004).
[70] M. Fitzgerald, R. R. Picard, and R. N. Silver, Europhys. Lett. **46**, 282 (1999).
[71] B. Smit, Mol. Phys. **85**, 153 (1995).